High Time Density Light Curves of

Six Short Period Variable Stars

Christiana Z Suggs

A senior thesis submitted to the faculty of
Brigham Young University
in partial fulfillment of the requirements for the degree of

Bachelor of Science

Eric G. Hintz, Advisor

Department of Physics and Astronomy

Brigham Young University

ABSTRACT

High Time Density Light Curves of
Six Short Period Variable Stars

Christiana Z Suggs
Department of Physics and Astronomy, BYU
Bachelor of Science

As part of our variable star follow-up program, we have examined a number of stars classified as δ Scuti variable stars by the ATLAS (Asteroid Terrestrial-impact Last Alert System) survey to verify if the classification is accurate. We inspected six different stars, ATO J070.9950+37.4038, ATO J328.8034+58.0406, TYC 3224-2602-1, ATO J086.0780+30.3287, ATO J077.6090+36.5619, and ATO J045.8159+46.0090, using the telescopes at Brigham Young University. We plotted the changes in brightness over time and performed a Fourier analysis on the data to examine the frequencies of pulsation. Comparing our frequencies to the ones published by other surveys confirmed the classification of these stars. While the published fundamental frequencies were very close to our own, phase curves using data from surveys like ATLAS, ASAS-SN and TESS often lacked subtle details found in the higher cadence data taken at BYU. While the other surveys can get accurate data points, the spacing between observations makes it difficult to run a rigorous analysis on the stars. We have established baseline measurements, times of maximum light, and ephemerides for each of the stars analyzed here. Future work is needed to determine the long term pulsation behavior of the stars.

Keywords: delta Scuti — stars: individual (ATO J070.9950+37.4038, ATO J328.8034+58.0406, TYC 3224-2602-1, ATO J045.8159+46.0090, ATO J345.4240+42.0479, ATO J086.0780+30.3287)

ACKNOWLEDGMENTS

Thanks to Dr. Hintz for all his help and guidance on this project.

Special thanks to the Brigham Young University Department of Physics and Astronomy for their continued support of research efforts and the Theodore Dunham, Jr. Grant for Research, which has been used to help equip the BYU campus observatory. This research was also supported in part by NASA through the American Astronomical Society's Small Research Grant Program.

This work makes use of data products from the Two Micron All-Sky Survey, which is a joint project of the University of Massachusetts and the Infrared Processing and Analysis Center/California Institute of Technology, funded by the National Aeronautics and Space Administration and the National Science Foundation.

Additional thanks to the variable star observations from the AAVSO International Database contributed by observers worldwide and used in this research.

Funding for the TESS mission is provided by NASA's Science Mission directorate.

This work has made use of data from the European Space Agency (ESA) mission *Gaia* (https://www.cosmos.esa.int/gaia), processed by the *Gaia* Data Processing and Analysis Consortium (DPAC, https://www.cosmos.esa.int/web/gaia/dpac/consortium). Funding for the DPAC has been provided by national institutions, in particular the institutions participating in the *Gaia* Multilateral Agreement.

Contents

List of Figures

List of Tables

Chapter 1

Introduction

1.1 δ Scuti Stars

As stars age, they transition from burning hydrogen to burning helium in their cores. At such transition points, stars can become unstable and periodically vary in size and temperature in an attempt to regain their equilibrium. By studying these transitioning stars, we can learn more about how stars evolve with time. Different types of stars experience different variations, so astronomers have sorted "variable stars" into categories based on their mass, age, period–how often they pulsate– and their change in brightness as they pulsate. One particularly interesting group is δ Scuti variable stars. These are stars with spectral type A and F that have recently completed the main hydrogen burning stage of their life. They experience pulsation over a matter of hours, compared to the months or years of other types of variable stars. Because these stars pulsate so quickly, they are easier to study since we can collect a lot of data about them in a short amount of time. The variation in δ Scuti stars is due to a shell of partially ionized atoms within the star that periodically trap and release heat. As the star contracts, the shell becomes ionized and opaque, trapping the heat coming from the center of the star. To maintain its equilibrium, the star begins to expand its radius. As it

expands, the shell becomes only partially ionized again, and the heat is allowed to escape from the star. Without the excess heat pushing the star to expand, the star begins to shrink in size (Carroll & Ostlie 2017).

We can investigate these periodic radius changes by measuring the brightness of a star over time. The resulting light curve allows us to calculate the main period and identify secondary frequencies, which indicate another level of complexity in the star's behavior. Analyzing the pulsation frequencies can tell us about the location of the partially ionized shells as well as telling us whether the star is pulsating radially or nonradially. We can also discover if the star is changing in time. As the star evolves, the pulsation period and amplitude can shift. Breger & Pamyatnykh (1998) discussed the possibility of tracing these changes to learn more about the star's evolution. This would allow us to more fully understand how stars transition between different stages in their lives. Breger (1979) explored the relation between the period of pulsation and the true brightness of δ Scuti stars. Since the brightness we measure is affected by the distance between us and a star, we can use the period to find the true brightness and compare it with what we measure to calculate the distance of the star from us. This allows us to get a better understanding of where these types of stars form in the galaxy.

1.2 Transient Event Surveys

The Asteroid Terrestrial-impact Last Alert System's (ATLAS, Heinze et al. (2019)) primary purpose is to find asteroids that might impact Earth. Each of the four telescopes in the system observes a quarter of the night sky four times every clear night, which allows them to detect moving asteroids. Due to this observing method, ATLAS can detect light variations and collect data on a number of objects whose light varies with time, including supernovae, variable stars, and eclipsing binary systems. There are other similar programs, such as the All Sky Automated Survey for SuperNovae

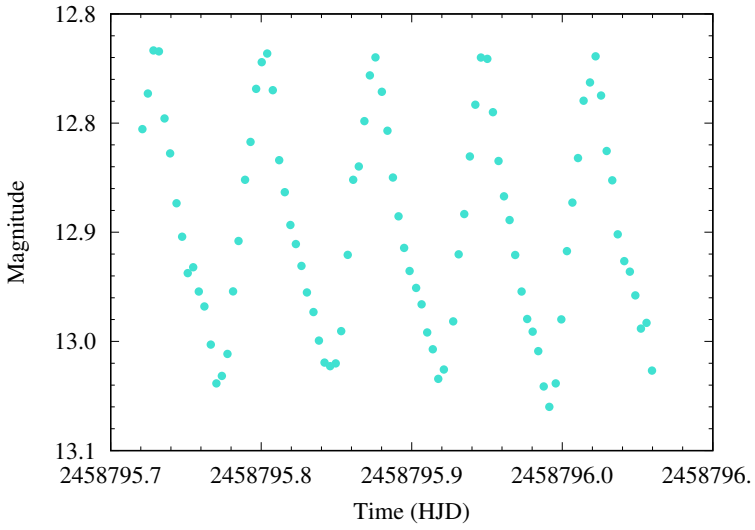

Figure 1.1 Data collected for ATLAS 59 on November 7, 2019.

(ASAS-SN, Shappee et al. (2014), Kochanek et al. (2017)) and the Transiting Exoplanet Survey Satellite (TESS, Ricker et al. (2015)), which use different filters and observation cadences to observe supernovae and transiting exoplanets, respectively. An observation cadence is how often measurements are taken, and different types of objects are best studied using different observation frequencies. For example, it is best to observe δ Scuti stars multiple times an hour to be able to clearly trace their changes in brightness. This can be seen in Figure 1.1, where the star ATO J086.0780+30.3287 (ATLAS 59) is observed 90 times over the course of 8 hours. Because the star's brightness is measured so frequently, we can clearly trace the variations in its brightness over time. For asteroid detection programs like ATLAS, observations need only be taken a few times a night. Despite the lower observation cadences, ATLAS, ASAS-SN, and TESS often observe and classify different variable stars due to their wide fields.

We are interested in the potential δ Scuti variables which have been found by these surveys. In a review of the known δ Scuti from 2000 (Rodríguez et al. 2000) we see that most of the stars are Low Amplitude δ Scuti (LADS), which rotate rapidly and have a number of nonradial low

amplitude pulsation modes. However, many of the new potential δ Scuti stars are High Amplitude δ Scuti (HADS), which only experience a few (generally radial) high amplitude pulsation modes. They also have a low rotational velocity, which is why their pulsation amplitude can be so big. The large number of new HADS stars could change our understanding of the ratio of the two δ Scuti subtypes. However, since programs like ATLAS, ASAS-SN, and TESS don't usually observe at the right cadence to provide good coverage for these short period variable stars, accurate classification can be challenging. But, misclassifications can lead to misinterpretations of the nature of δ Scuti stars. This calls for a more in depth analysis of these stars to verify if they are indeed HADS.

1.3 Stars Analyzed

From ATLAS we find three lists where potential δ Scuti variables might be found, the PULS, MPULS and SINE lists (Heinze et al. 2019). These represent targets classified as pulsating (PULS), multi-periodic pulsating (MPULS) and sine shaped curves (SINE). As mentioned above, we want to give a more complete classification than what is provided by ATLAS. We started with the ATLAS database of potential δ Scuti stars (Heinze et al. 2019) and selected objects to examine more closely. The resulting analysis for six of the targets will be presented here. We have renamed each star according to our own internal numbering system. (See Table 1.1)

ATLAS 1 was analyzed (Christy et al. 2023) as part of a larger survey identifying variable stars from ASAS-SN g band photometry. TESS has performed some additional analysis of ATLAS 8 (Jenkins et al. 2016), finding a primary period of 0.266 days and a secondary period of 0.088 days. There is some question as to whether this star has a planet orbiting around it, but as of yet there is not enough data to come to any certain conclusion. All of the stars except for ATLAS 63 were classified as HADS, but ATLAS 63 was simply classified as a δ Scuti star by ASAS-SN and the American Association of Variable Star Observers (AAVSO) due to its lower pulsation amplitude.

Table 1.1. Stars Analyzed

BYU Name	Object Name	RA	Dec.	ASAS-SN Published Period (days) Magnitude (V Filter) Amplitude	AAVSO Published Period (days) Magnitude
ATLAS 1	ATO J070.9950+37.4038	04:43:58.796	+37:24:14.123	0.094387 11.83 0.3	0.0943878 12.32+/-0.35 g
ATLAS 4	ATO J328.8034+58.0406	21:55:12.840	+58:02:26.306	0.1946479 11.77 0.24	
ATLAS 8	TYC 3224-2602-1	23:01:41.8	+42:02:52.7	0.0886644 11.66 0.19	0.0886621 11.55 - 11.81 V
ATLAS 59	ATO J086.0780+30.3287	05:44:23.3	+30:20:44	0.072821 12.87 0.3	0.0728218 12.67 - 13.0 V
ATLAS 63	ATO J077.6090+36.5619	05:10:26.175	+36:33:43.086	0.0702774 13.1 0.1	0.072775 13.374+/-0.124 g
ATLAS 75	ATO J045.8159+46.009	03:03:13.2	+46:01:59	0.0855426 13.01 0.26	0.0855422 13.224+/-0.410 g

As part of our program studying short period pulsating variable stars such as δ Scuti, we explore a number of topics related to these relatively newly discovered variable stars. First, we compare the period determination from the ATLAS, ASAS-SN, and TESS surveys with our own time series observations. We next establish baseline measurements for these stars that allow for future monitoring and more fully classify each object. We then present an Observed minus Calculated (O-C) period determination for each of these δ Scuti stars by fitting a linear model to the main pulsation frequency to determine if the period is consistent. Finally, we report a Fourier decomposition of the light curves, and compare the period found from our own data to the periods found from archival data. We find that although the ATLAS program did classify each of the analyzed stars correctly, the observations were spaced too far apart to perform an in depth investigation on these δ Scuti stars. The data we took at Brigham Young University (BYU) was much more effective at performing an initial analysis of each of the six stars studied.

Chapter 2

Methods

Here, we shall describe our measurements of the six δ Scuti stars, and our subsequent analysis of their pulsation periods. We obtained an equation to describe the times of maximum light of the stars and ran a Fourier decomposition on the data to examine all the frequencies found in the light curves. We compared our results to those found from the ATLAS, ASAS-SN, and TESS surveys, and find them to be in agreement with each other.

2.1 Photometric Data

We collected data on the stars from 2019 to 2022 using the BYU telescopes and obtained data from ATLAS, ASAS-SN, and TESS using the online archives for each survey.

2.1.1 Robotic Observations

We observed each of the six δ Scuti stars using the 6", 8", 10", and 12" telescopes of the Orson Pratt Observatory on the Brigham Young University campus. The 6" telescope is a TPO 6" telescope with a 953 mm focal length, a ML 8300 CCD camera, and a 5.4 x 5.4 μm pixel size after binning. The

Table 2.1. Nights Observed for All ATLAS Objects

Object	Obs Start	Obs End	Days Observed	Hours Observed	# Observations
ATLAS 1	Sept 2019	Oct 2022	33	95.59	2307
ATLAS 4	Sept 2020	Dec 2021	33	179.01	4142
ATLAS 8	Sept 2019	Aug 2022	11	32.01	504
ATLAS 59	Nov 2019	Nov 2019	6	36.13	401
ATLAS 63	March 2020	Feb 2022	9	22.31	387
ATLAS 75	Aug 2019	Sept 2019	7	30.53	247

8" telescope is a Vixen VMC200L telescope with a 1950 mm focal length. The 10" is a Takahashi Mewlon 250mm telescope with a focal length of 3000 mm. The 12" telescope is a TPO 12" with a focal length of 2440 mm. Each of the telescopes (except for the 6") used a FLI ML8300 CCD camera with a 10.8 x 10.8 μm pixel size after binning. Note that the 8" telescope used a FLI ML3200 CCD with a 13.6 x 13.6 μm pixel size after binning before September 2022.

Data was taken through a Johnson V filter, which measures light at 540 nm. Table 2.1 lists how many times each object was observed, as well as when this data was gathered. Additional data was taken with g and R filters, but that data will not be analyzed here.

Along with direct observations of the stars with the V filter, we took calibration shots to determine the noise in our data. We used the program IRAF to subtract errors due to machinery and the atmosphere in order to only look at the brightness of each star in the shot. We then used the program AstroImageJ (Collins et al. 2017) to extract the brightness of each star in the field of view for every observation. Whenever possible, we selected stars with known magnitudes in SIMBAD to use as calibration stars. Those stars allowed us to calibrate enough comparison stars to provide a solid baseline for our variable star. By comparing the brightness of the variable star to the baseline, we obtain a clear light curve, as seen in Figure 1.1.

For ATLAS 59, we used two stars in the field (Figure 2.1) documented in SIMBAD to calibrate

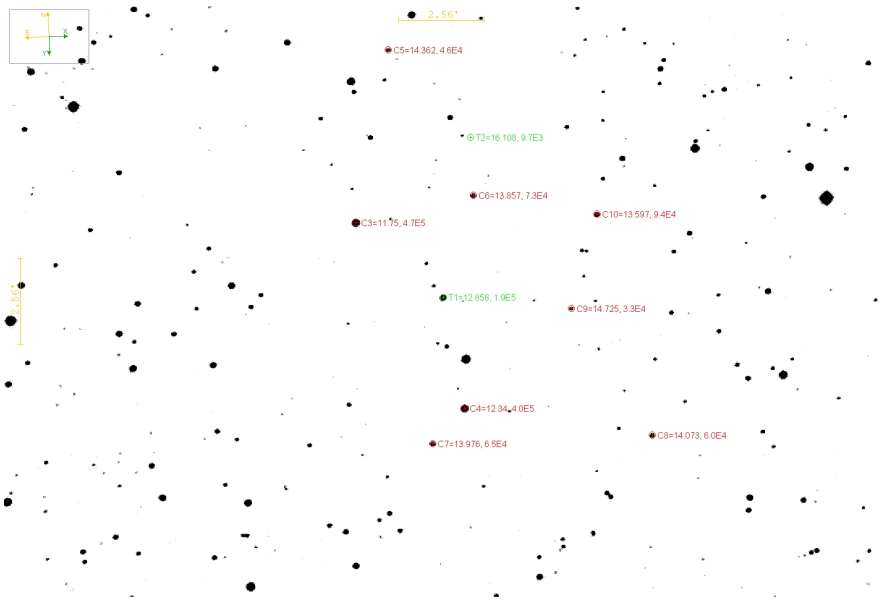

Figure 2.1 Field of ATLAS 59 (labeled T1) with comparison stars C3-C10. T2 is another variable star and was not used as a comparison star.

Table 2.2. ATLAS 59 Comparison Stars

Star	RA	Dec.	V	σ_m
C3 (TYC 2405-1658-1)	05:44:30.16	+30:22:06.60	11.75	n/a
C4 (TYC 2405-1468-1)	05:44:16.64	+30:16:23.74	12.34	n/a
C5	05:44:24.25	+30:27:11.30	14.362	0.003
C6	05:44:13.73	+30:22:42.14	13.857	0.001
C7	05:44:21.40	+30:15:23.85	13.976	0.002
C8	05:43:51.02	+30:15:15.28	14.073	0.002
C9	05:44:01.13	+30:19:09.93	14.725	0.003
C10	05:43:56.79	+30:21:55.54	13.597	0.001

the comparison stars C5-C10. The average brightness of each comparison star for ATLAS 59 is reported in Table 2.2, and a sample night of data is found in Figure 1.1.

Table 2.3. Archival Data (Number of observations collected)

Data Set	ATLAS 1	ATLAS 4	ATLAS 8	ATLAS 59	ATLAS 63	ATLAS 75
ATLAS c filter	139	96	98	192	149	141
ATLAS o filter	54	47	134	147	138	145
ASAS-SN V filter	542	620	626	1318	558	584
ASAS-SN g filter	1009	1529	1330	2908	1091	1184
TESS	812	1740	697	10896	777	867

We followed a similar procedure for each ATLAS object, carefully selecting comparison stars that do not appear to have a variable nature. Note that we shall use ATLAS 59 as a representative star for the analysis presented here, but corresponding information for each δ Scuti star can be found in Appendix A.

2.1.2 Archival Photometry

We downloaded data from the ATLAS, ASAS-SN, and TESS online archives to compare with our own observations. The data from the ATLAS program was downloaded using the NASA MAST archive. These observations are in two filters, *c* and *o*, which measure light at 420–650 nm and 560–820 nm, respectively. Because these cyan and orange filters don't observe the same wavelengths as our *V* filter, we can't directly compare the data since the brightness measured will be different. However, the period of pulsation will be the same regardless of the filter. We did a search for the last 3000 days within the ASAS-SN archive to find data on each δ Scuti star. Data from ASAS-SN can be either in a *V* or *g* filter. We also downloaded data from the TESS archive. This data comes from a fairly wide filter centered roughly in the *I* band at 786.5 nm. The number of data points collected from each survey is listed in Table 2.3

2.2 Analysis

Now that we have mapped out how each star's light changes in time, we are able to identify the peaks, or times of maximum light. These times allow us to construct an O-C diagram, which shows if the pulsation is consistent or the period is changing. We also performed a Fourier decomposition to extract the different frequencies from the light curve.

2.2.1 Times of Maximum Light

We used the program Peranso (Paunzen & Vanmunster 2016) to identify the times of maximum light from the BYU data. We were able to extract additional times of maximum light from the AAVSO archive data for ATLAS 8 and 59, and from TESS data for ATLAS 4 and 59.

To closely match the star's behavior, we fit a fifth order polynomial equation to the light curve segment around each maxima and obtained the time of maximum brightness from the fit. The number of maximums found for each star are gathered in Table 2.4. We used these maximums to determine an ephemeris, or a linear fit equation used to measure how constant the period is, which is also found in Table 2.4. The errors included in parentheses are for the last two digits of both the period and starting epoch. The TESS data for ATLAS 59 taken in November 2019 had 30 minute exposures, which was too low of a cadence to be able to extract times of maximum light. Data taken from September to November of 2021 only had 10 minute exposures, so we were able to resolve 959 times of maximum light for ATLAS 59. These times were well after the 20 times of maximum light extracted from the BYU data (see Table 2.5) so we used the TESS observations to estimate an initial ephemeris. We then extrapolated backwards to determine the cycle number for the BYU data points, which allowed us to refine our overall ephemeris equation.

Using this equation we predicted when the times of maximum light should be and compared them with what was observed to obtain Observed minus Calculated (O-C) values for each maximum.

Table 2.4. Times of Maximum Light and Ephemerides

Star	Times of Max Light	Ephemeris
ATLAS 1	34	$\text{HJD}_{\text{max}} = 2458757.98212(35) + 0.094387573(43)E$
ATLAS 4	231	$\text{HJD}_{\text{max}} = 2458739.46173(47) + 0.194646242(46)E$
ATLAS 8	13	$\text{HJD}_{\text{max}} = 2458760.62172(15) + 0.088657650(29)E$
ATLAS 59	979	$\text{HJD}_{\text{max}} = 2459474.21365(15) + 0.072822388(10)E$
ATLAS 63	19	$\text{HJD}_{\text{max}} = 2458914.65523(50) + 0.070277624(98)E$
ATLAS 75	13	$\text{HJD}_{\text{max}} = 2458726.96546(69) + 0.0855459(39)E$

The O-C values for the BYU data for ATLAS 59 are also gathered in Table 2.5 and in Figure 2.2 we show its O-C diagram, including both BYU and TESS O-C values. The gap is due to the time skip between when the data was taken. Note that the O-C values are very small, which means that our calculated period is very close to the actual period of the star. There was no appreciable trend in the values over time. A trend in the values would indicate that the period is increasing, decreasing, or has an abrupt shift. Because there is no trend for any of δ Scuti stars analyzed, the period for each of the stars is unchanging over the observed time span.

2.2.2 Fourier Decomposition

The fundamental period for ATLAS 59 was determined by Peranso to be 0.072818(35) days with an average magnitude of 12.94999. This value agrees well with the ephemeris value calculated from the times of maximum light (0.072822(39)). Figure 2.3 shows that our calculated period can accurately phase the BYU, ATLAS, ASAS-SN, and TESS data. Since we have obtained such a clean phase plot, we can see that the calculated period is consistent across all data sets, though we note that we are able to see the most details in the BYU phase curve due to the high cadence of the data.

Table 2.5. BYU Times of Maximum Light for ATLAS 59

Cycle	HJD 2450000.0+	$O-C$	Source
0	8795.72877	-0.00001	BYU
1	8795.80196	0.00035	BYU
2	8795.87482	0.00039	BYU
3	8795.94747	0.00022	BYU
4	8796.01987	-0.00020	BYU
14	8796.74755	-0.00074	BYU
15	8796.82107	-0.00004	BYU
16	8796.89400	0.00007	BYU
17	8796.96654	-0.00022	BYU
18	8797.04031	0.00074	BYU
28	8797.76821	0.00042	BYU
29	8797.84019	0.00043	BYU
30	8797.91338	-0.00006	BYU
31	8797.98640	0.00015	BYU
56	8799.80628	-0.00052	BYU
57	8799.87889	-0.00073	BYU
58	8799.95232	-0.00012	BYU
59	8800.02566	0.00040	BYU
124	8804.76001	0.00135	BYU
125	8804.83048	-0.00100	BYU

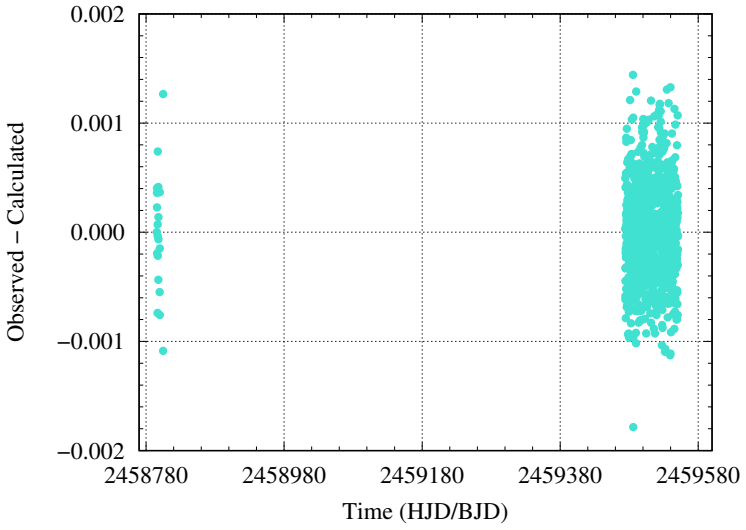

Figure 2.2 O-C Diagram for ATLAS 59 from 979 times of maximum light.

To further investigate the stars' behavior, we used the program Period04 (Lenz & Breger 2005) to perform a Fourier decomposition of the data. We found all frequencies with a signal to noise ratio greater than 5, since below this point the detected frequencies are more due to noise than any real trends in the data.

As seen in Table 2.6, Period04 found the main frequency of ATLAS 59 to be 13.73509 cycles/day and found 3 multiples of this same frequency in the BYU data. The main frequency is again in good agreement with the calculated ephemeris. The ASAS-SN data gives the same frequencies, but the ATLAS and 2019 TESS data are unable to detect more than the main frequency and one multiple. The TESS data from 2021 was able to detect four multiples of the fundamental frequency, in addition to five other frequencies. This indicates that there is a lot of information to be found in short cadence data that is missed in longer observations.

The phase diagrams and period analysis for each of the other stars can be found in Appendix A. Most of the calculated periods were consistent, but exceptions will be discussed in the Results section.

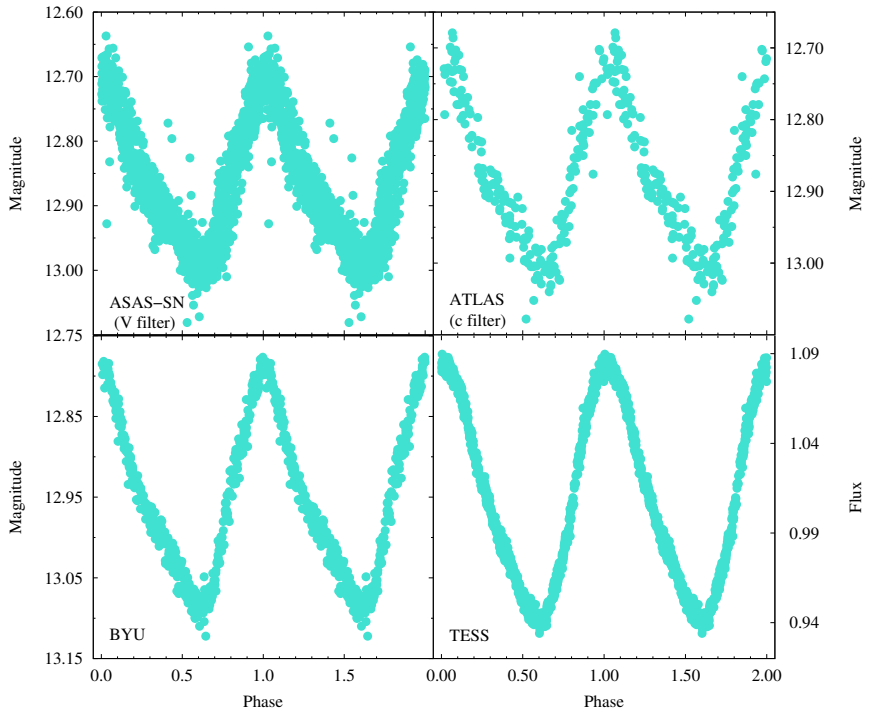

Figure 2.3 Phased Data for ATLAS 59 from BYU, ATLAS, ASAS-SN, and TESS using the calculated period

Table 2.6. Frequency Content of ATLAS 59

Survey		Frequency c d^{-1}	Amplitude mag	S/N
BYU	f_1	13.73509	0.12901	75.4
	$2f_1$	27.46472	0.03278	38.5
	$3f_1$	41.21620	0.00726	6.4
	$4f_1$	54.92452	0.00715	11.0
ASAS-SN (V filter)	f_1	13.73227	0.13112	127.5
	$2f_1$	27.46457	0.03426	34.3
	$3f_1$	41.19683	0.00678	7.0
	$4f_1$	54.92922	0.00596	6.3
ASAS-SN (g filter)	f_1	13.73208	0.15120	136.1
	$2f_1$	27.46417	0.03782	34.6
	$4f_1$	54.92839	0.00743	7.5
	$3f_1$	41.19625	0.00634	5.9
ATLAS (c filter)	f_1	13.73230	0.13286	47.9
	$2f_1$	26.46196	0.02959	12.4
ATLAS (o filter)	f_1	13.73239	0.09564	28.3
	$2f_1$	27.46459	0.02792	11.1
TESS (2019)	f_1	13.73005	0.06768	235.4
	$2f_1$	27.46118	0.01137	67.2
	f_2	47.96606	0.00207	5.8
TESS (2021)	f_1	13.73189	0.07532	878.88393
	$2f_1$	27.46379	0.01953	284.83656
	$3f_1$	41.19636	0.00407	73.98008
	$4f_1$	54.92825	0.00329	50.83216
	f_2	17.67071	0.00212	27.98305
	f_3	68.66045	0.00203	37.95629
	f_4	3.93751	0.00108	14.53443
	f_5	31.40195	0.00087	17.49675
	f_6	61.59736	0.00078	13.82514

Chapter 3

Results

From our analysis of six δ Scuti stars, we were able to confirm their published periods and classifications. We also established baseline measurements and determined times of maximum light. While we are able to learn a lot about δ Scuti stars in a short amount of time due to their rapid pulsations, more information is needed to fully classify these stars and to understand their long term behavior.

3.1 Pulsation Modes and Classification

To further check the designation of these objects we calculated their Q values as detailed in Breger (1990), where Q is a pulsation constant that depends on the mode the star is pulsating in. To find this value we acquired data from the Gaia EDR3 release (Bailer-Jones et al. 2021), which is gathered into Table 3.1. In addition to the six targets from this paper we include an additional ATLAS target reported in Hintz et al. (2022) that we label as ATLAS 30. According to Breger (1979), the Q values for ATLAS 8, ATLAS 30, ATLAS 59, and ATLAS 75 indicate that they are pulsating in the fundamental or base frequency. In Figure 3.1 we show the Period-Luminosity (PL) relations for each of our δ Scuti variables as detailed in Poro et al. (2021). The four lines in the figure represent

Table 3.1. Information from Gaia EDR3 and Determined Q value.

Target	l	b	T_{eff}	$\log g$	distance	Q
	$^\circ$	$^\circ$	K		pc	
ATLAS 1	165.6045505	-5.5230815	6846	3.488	678	0.023
ATLAS 4	101.3089148	2.7693820	6836	3.277	1078	0.030
ATLAS 8	102.0447991	-16.3297311	7099	3.876	764	0.033
ATLAS 30	133.9849359	-8.2950934	9756	4.010	1041	0.030
ATLAS 59	178.6639644	0.4848620	7086	3.825	999	0.028
ATLAS 63	169.5566574	-1.9089473	7014	3.523	1567	0.015
ATLAS 75	145.5688619	-10.9884367	7181	3.794	1365	0.027

the PL relations for fundamental pulsators (blue), 1st overtone (green), 2nd overtone (red), and 3rd overtone (purple). In addition to having Q values that indicate fundamental pulsation, most of our targets lie near the PL relation for fundamental pulsators. ATLAS 63 is the only exception, lying near the first overtone relation instead. More data is needed to investigate this different behavior.

To verify our calculations, we can examine the GALExtin maps (Amôres et al. 2021), which estimate interstellar extinction for a given location based on 2D and 3D maps and models. These maps indicate that there is likely a larger amount of extinction in the direction of ATLAS 59, which would move it closer to the fundamental line in Figure 3.1 – additional evidence that our calculations were correct. In addition, if we consider the δ Scuti instability strip from Breger (1979) we find that all seven of our targets are near the red edge of the instability strip, which further confirms our classification of these stars.

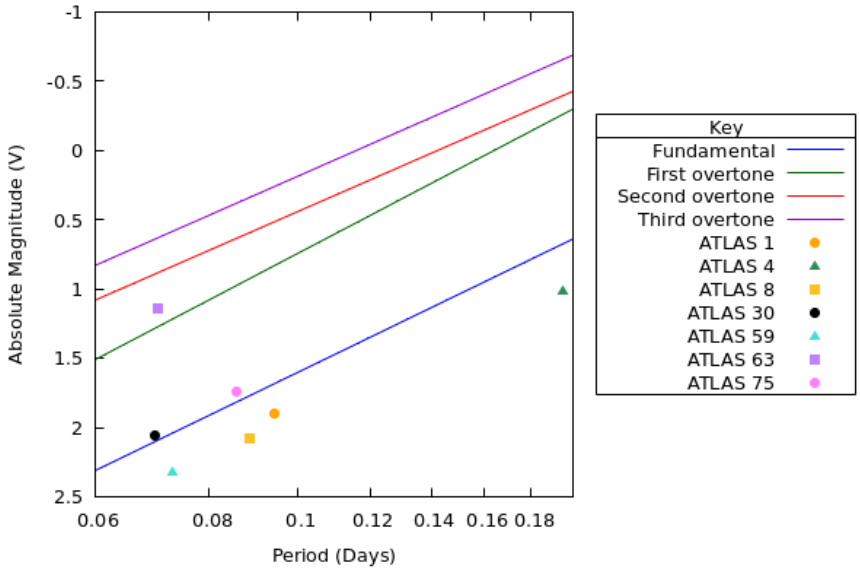

Figure 3.1 Period-Luminosity relations from Poro et al. (2021). Lines represent period-luminosity relations for fundamental pulsators (blue), 1st overtone (green), 2nd overtone (red), and 3rd overtone (purple).

3.2 Survey Comparison

For each of the δ Scuti stars analyzed, the main period Period04 found from the BYU data agrees well with published values. The program sometimes struggled to find higher order frequencies from the ATLAS survey due to the fact that there often aren't enough data points in a given night to clearly observe such fast pulsators. There are at most five or six points in a light curve, which makes it difficult to identify subtle features in the pulsation. It is also challenging to generate a clean phase diagram for ASAS-SN due to the large amount of noise in the data. This is because the ASAS-SN program is made up of an array of 24 different telescopes set up around the globe, which makes it hard to have consistent observing conditions. We can sometimes find higher order frequencies from TESS, but the data is subject to biases from its observing cadence. Until recently, TESS would take a full frame image (FFI) every 30 minutes, which documents a wide area of the sky. While this is a relatively fast cadence, it is sometimes insufficient to get good light curves for the shorter

period stars like ATLAS 59. For ATLAS 4, which has a slightly longer period, TESS was able to provide many times of maximum light and identify a large number of higher order frequencies, as can be seen in Table A.7 of Appendix A. As TESS's cadence has increased in past few years, we can now use it more for the shorter period variable stars, as seen from our discussion of ATLAS 59 earlier. We do need to be wary of relying too heavily on the frequencies detected by TESS, since it observes a sector of the sky for 27.4 days before moving on, which means that there might be some observational bias in the frequencies detected. Observation bias comes from monitoring an object in a periodic manner that may introduce additional frequencies in the data. For example, observing an object once a night can cause a false one-day frequency to be detected. Additionally, the relatively short observation span makes it difficult for us to detect long term behavior from TESS data.

3.3 Additional Times of Maximum Light

As with ATLAS 59, we used the period calculated in the ephemeris equation to phase the data from each of the surveys. The ephemeris equation is:

$$\mathrm{HJD} = \mathrm{HJD_o} + \mathrm{P} * \mathrm{E} \tag{3.1}$$

Where HJD is the current date, $\mathrm{HJD_o}$ is the date where the cycle begins, P is the period of the oscillations, and E is the cycle number and phase. As seen from the figures in Appendix A, most of the surveys phased together quite well, indicating that the period is unchanging over the time span of each survey. However, for ATLAS 8 and ATLAS 75, the ATLAS and ASAS-SN survey data do not phase very well with the calculated ephemeris. (See Figure 3.2)

This indicates that the period has not stayed constant, contrary to what our O-C diagrams indicate. This is because our diagrams only document the period over the time we observed at BYU. Unfortunately, no times of maximum light can be extracted from the ASAS-SN and TESS surveys

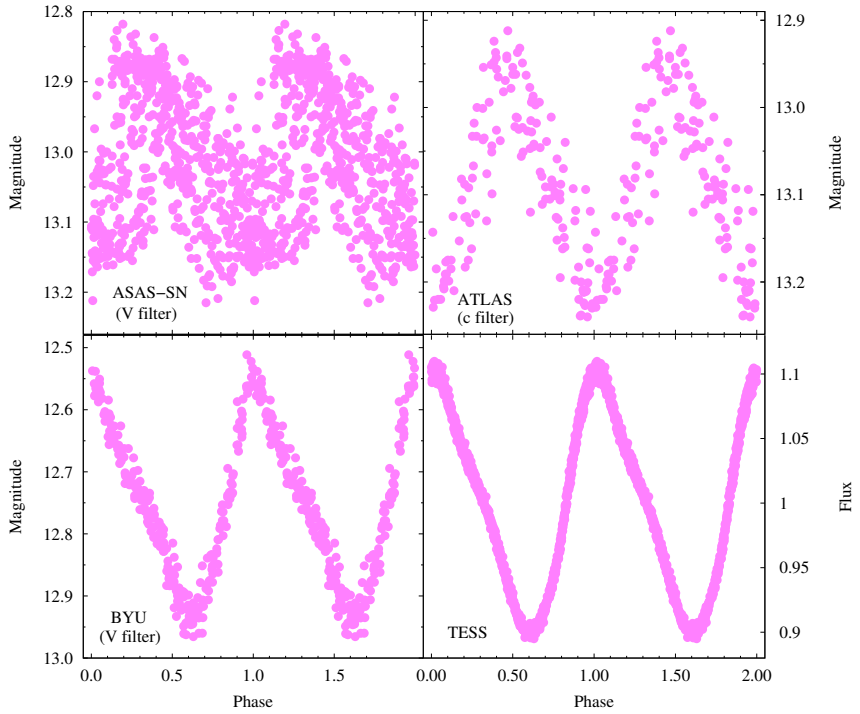

Figure 3.2 Phased Data for ATLAS 75 from BYU, ATLAS, ASAS-SN, and TESS using the calculated period from the ephemeris. Note that while the BYU and TESS data phase well, the ATLAS and ASAS-SN data do not phase into a clean light curve with the calculated period

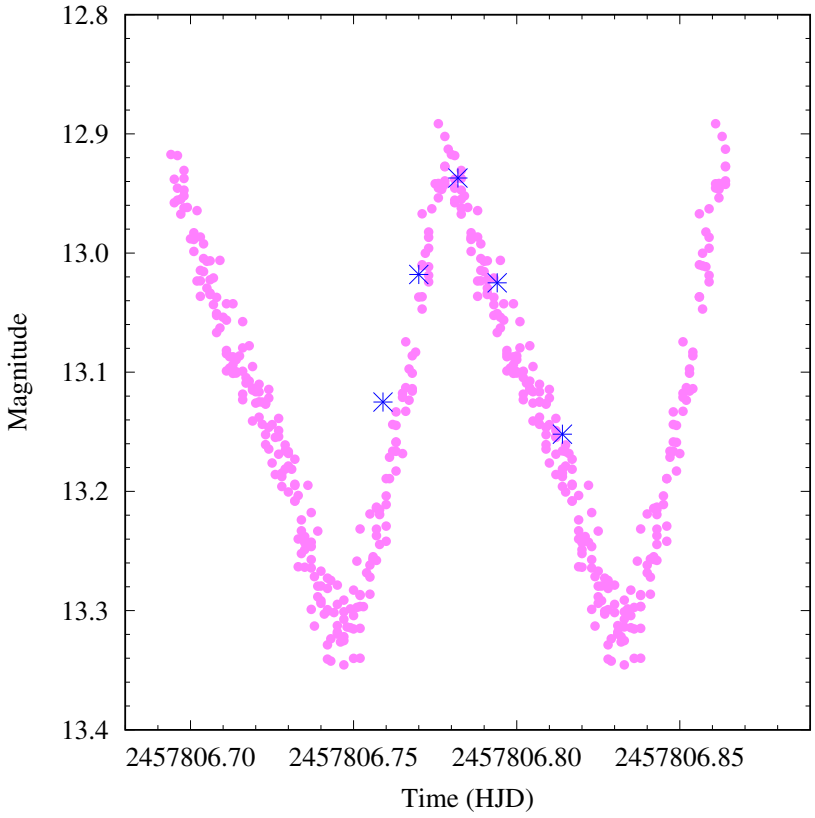

Figure 3.3 The BYU model for ATLAS 75 is shown here in pink while the ATLAS data it was fitted to is shown in blue

to generate a comprehensive O-C diagram and confirm whether the period is changing with time. To remedy this, we used the phased BYU data as a model and manually adjusted the phase (E) and the magnitude of the model to fit with the available ATLAS and ASAS-SN data points for a given night. We then calculated the time of maximum light from the model. Figure 3.3 shows that our model does a fair job of filling in the gaps in the data. However, for this method to be useful, we need to perform the modeling in a more statistically rigorous way, instead of manually adjusting the parameters and visually fitting the curve. Further work will determine if using the model is an effective way to generate additional times of maximum light, which can then help determine the long term behavior of the star.

3.4 Conclusions and Future Work

After analyzing six δ Scuti variable stars, we find that ATLAS correctly classified the stars, but does not observe them at the right cadence to fully understand their behavior. The correct classification may not be surprising considering that these stars are HADS, so they have dramatic and thus more easily detected fundamental pulsations. They are also mostly monoperiodic, which adds to the ease of classification. While we can get further information on the stars from other surveys, more frequent observations with a better signal to noise ratio are needed to exactly model the behavior. Here, we established baseline measurements, times of maximum light, and ephemerides for each of these stars.

Of all of the stars analyzed here, ATLAS 4 has the most complicated behavior. While the fundamental period does not appear to change over time, there are many higher order periods detected. This could be because ATLAS 4 is just a more complicated object, but it could also be due to the fact that it was observed for much longer than the other stars examined here. Long term observations of each of the six stars are needed to learn if they experience standard pulsations or if there is odd pulsation behavior which might indicate the presence of a stellar companion or change our understanding of these stars.

We also need more data to be able to map out the long term evolution of these stars. We might be able to use models to extract more information from surveys like ATLAS, but this method must first be verified. Additionally, there is some data available from the new James Webb Space Telescope on these stars. This powerful telescope generates detailed stellar spectra, which can tell us a lot about the chemical composition of the outer layer of these stars. By analyzing this, we can more accurately model the interior processes of the stars and better understand their current state. As we continue to analyze these stars, we can draw conclusions about their normal behavior and learn how δ Scuti stars work in general. This can help us better understand how different types of stars evolve in time and bring us a step closer to understanding our universe.

Appendix A

Additional Figures and Tables

A.1 ATLAS 1

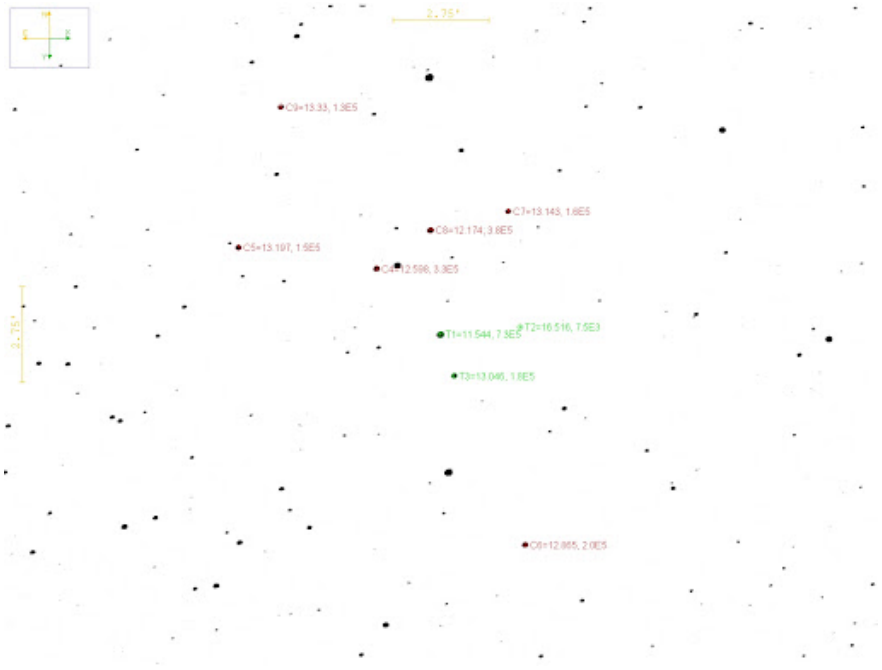

Figure A.1 Field of ATLAS 1 (labeled T1) with comparison stars C4-C9. T2 and T3 denote other variable stars in the field. C4 was used to calibrate the other comparison stars.

Table A.1. ATLAS 1 V Filter Comparison Stars

Star	RA	Dec.	Magnitude	Std. deviation
C4	04:44:07.8978344160	+37:26:08.642883660	12.598	n/a
(UCAC4 638-019207)				
C5	04:44:27.88	+37:26:47.42	13.197	0.020
C6	04:43:47.00	+37:18:09.68	12.865	0.018
C7	04:43:48.79	+37:27:43.91	13.143	0.020
C8	04:44:00.08	+37:27:13.46	12.174	0.014
C9	04:44:21.54	+37:30:48.26	13.330	0.018

Table A.2. Nights Observed for ATLAS 1

Date	Start Time (HJD)	End Time (HJD)	Length (hrs)	# Observations	Telescope
Sept 30, 2019	2458757.927533	2458758.002111	1.789872	45	8"
Oct 2, 2019	2458759.875545	2458759.998321	2.946624	75	8"
Oct 3, 2019	2458760.872544	2458760.998179	3.015240	72	8"
Oct 5, 2019	2458762.879421	2458763.001490	2.929656	75	8"
Oct 6, 2019	2458763.873095	2458764.013753	3.375792	36	8"
Oct 10, 2019	2458767.865894	2458768.004746	3.332448	85	8"
Oct 11, 2019	2458768.874772	2458769.015987	3.389160	85	8"
Oct 14, 2019	2458771.866801	2458772.007539	3.377712	85	8"
Oct 23, 2019	2458780.857118	2458780.995632	3.324336	85	8"
Oct 24, 2019	2458781.858664	2458782.055422	4.722192	119	8"
Oct 25, 2019	2458782.845613	2458782.856771	0.267792	8	8"
Nov 10, 2019	2458798.652812	2458798.808962	3.747600	61	10”
Nov 11, 2019	2458799.891814	2458800.065731	4.174008	75	10”
Feb 11, 2020	2458891.631843	2458891.656147	0.583296	10	10”
Oct 29, 2021	2459517.705639	2459517.803000	2.336664	54	12"
Feb 13, 2022	2459624.612908	2459624.780379	4.019304	88	12"
Feb 18, 2022	2459629.617990	2459629.738305	2.887560	63	12"
Feb 19, 2022	2459630.618587	2459630.790587	4.128000	89	12"
Feb 28, 2022	2459639.613557	2459639.737069	2.964288	65	12"
Mar 24, 2022	2459663.610178	2459663.737193	3.048360	127	12"
April 6, 2022	2459676.618877	2459676.719789	2.421888	105	12"
Sept 23, 2022	2459846.916678	2459847.029687	2.712216	53	8"
Sept 25, 2022	2459848.903868	2459849.032980	3.098688	58	8"
Oct 3, 2022	2459856.898177	2459857.032678	3.228024	62	8"
Oct 4, 2022	2459857.875511	2459858.038292	3.906744	76	8"
Oct 6, 2022	2459859.865094	2459860.034605	4.068264	80	8"
Oct 10, 2022	2459863.847646	2459864.031594	4.414752	128	8" and 12"
Oct 12, 2022	2459865.878867	2459866.046487	4.022880	79	8"
Oct 17, 2022	2459870.973177	2459871.049770	1.838232	36	8"
Oct 20, 2022	2459873.965632	2459874.053167	2.100840	82	8"

Table A.2 (cont'd)

Date	Start Time (HJD)	End Time (HJD)	Length (hrs)	# Observations	Telescope

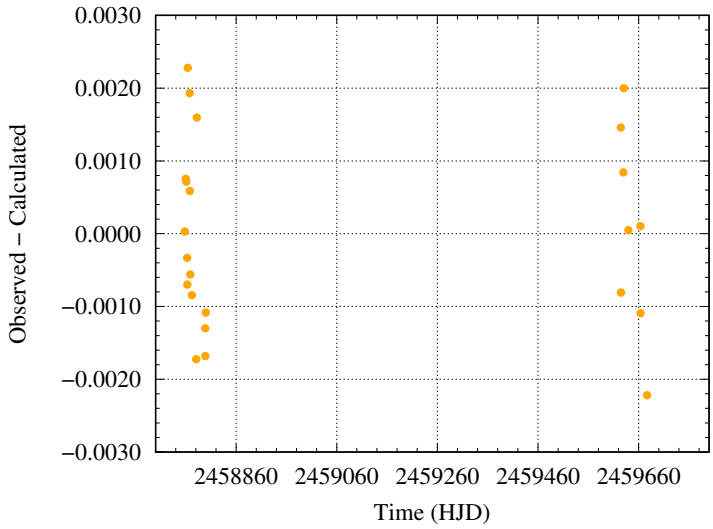

Figure A.2 O-C Diagram for ATLAS 1 from 34 times of maximum light. Note that the large gap in the middle is due to the fact that ATLAS 1 was not consistently monitored over during its 3 year observation period

Table A.3. Times of Maximum Light for ATLAS 1

Cycle	HJD 2450000.0+	$O-C$
0	8757.98218	0.00003
21	8759.96504	0.00075
31	8760.90888	0.00072
52	8762.88997	-0.00033
53	8762.98399	-0.00070
63	8763.93085	0.00228
105	8767.89478	0.00193
106	8767.98782	0.00588
116	8768.93055	-0.00056
148	8771.95066	-0.00084
243	8780.91660	-0.00172
254	8781.95818	0.00160
431	8798.66188	-0.00130
432	8798.75589	-0.00168
445	8799.98353	-0.00108
9182	9624.65010	0.00146
9183	9624.74222	-0.00081
9235	9629.65202	0.00084
9246	9630.69144	0.00200
9341	9639.65631	0.00005
9595	9663.63080	0.00010
9596	9663.72399	-0.00109
9733	9676.65396	-0.00222

Table A.4. Frequency Content of ATLAS 1

Survey		Frequency c d^{-1}	Amplitude mag	S/N
BYU	f_1	10.59464	0.14280	101.17587
(V filter)	$2f_1$	21.18924	0.02402	17.00163
	f_2	13.91049	0.00892	9.2211
	f_1	10.59464	0.15275	101.35127
ASAS-SN	$2f_1$	21.18928	0.02644	17.43796
(V filter)	f_2	7.18985	0.00887	5.85491
	f_3	31.78394	0.00850	5.6701
ASAS-SN	f_1	10.59462	0.16757	66.62587
(g filter)	$2f_1$	21.18923	0.02984	12.55534
	f_2	2.00545	0.01570	6.49536
ATLAS	f_1	10.59456	0.14254	41.27565
(c filter)	$2f_1$	21.18915	0.02785	12.75014
ATLAS	f_1	10.59477	0.10997	14.62622
(o filter)				
	f_1	10.59310	0.09283	669.74531
	$2f_1$	21.18795	0.01432	88.61506
	f_2	7.18893	0.00782	89.80706
	f_3	0.23047	0.00553	16.55931
	f_4	0.02749	0.00389	11.85352
	f_5	13.90810	0.00387	40.71922
TESS	f_6	16.21278	0.00283	20.03008
	f_7	0.46728	0.00246	7.98417
	f_8	3.59447	0.00120	17.49252
	f_1	10.08565	0.00210	15.61716
	f_9	14.37961	0.00147	15.49516
	f_{10}	3.31537	0.00146	12.07984
	f_{11}	23.49475	0.00089	9.09388

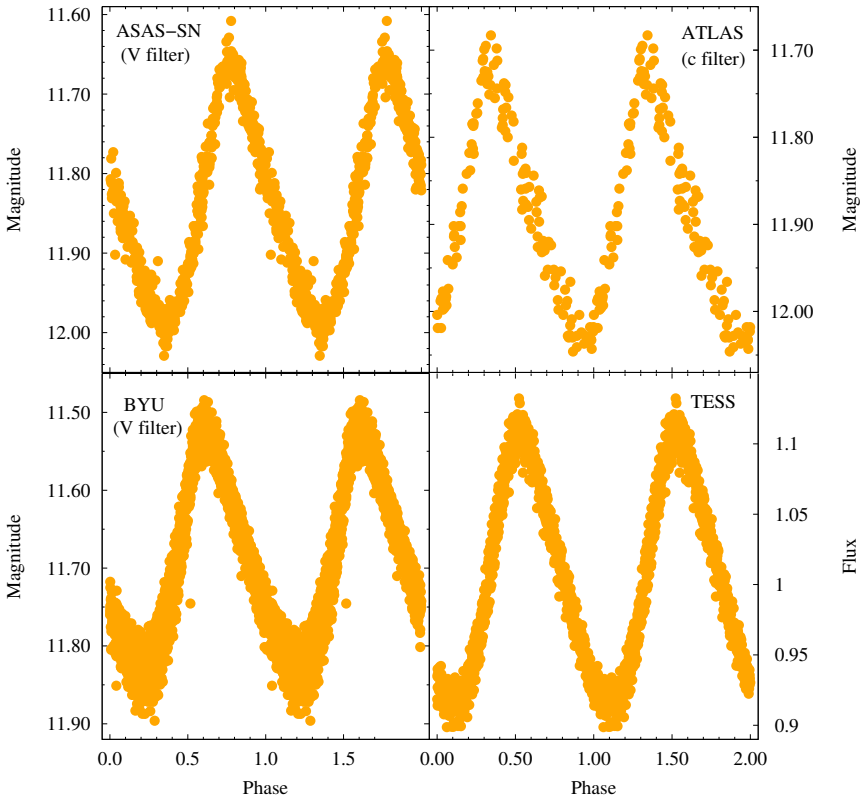

Figure A.3 Phased Data for ATLAS 1 from BYU, ATLAS, ASAS-SN, and TESS using the calculated period

A.2 ATLAS 4

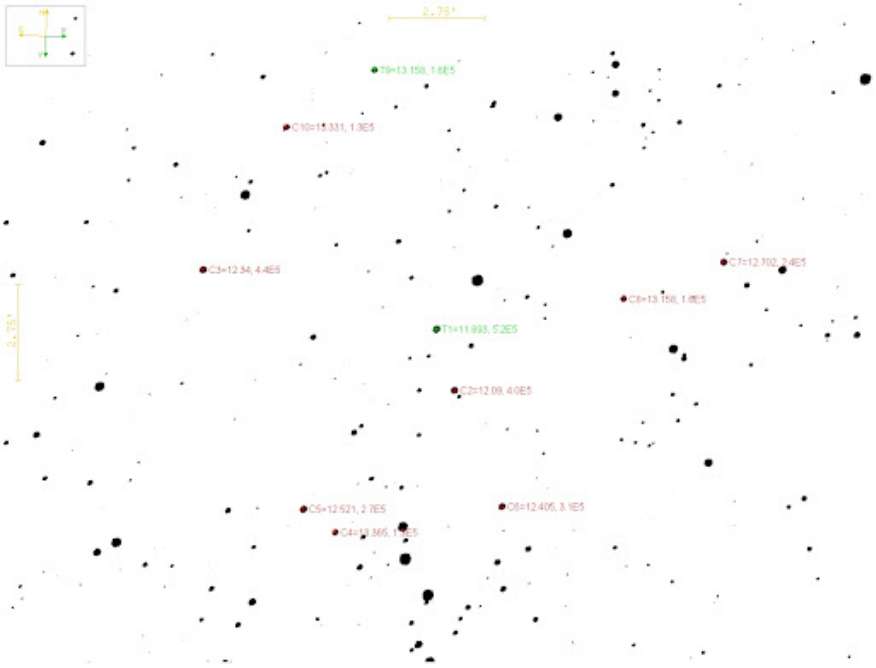

Figure A.4 Field of ATLAS 4 (labeled T1) with comparison stars C2-C8 and C10. C2 and C3 were used to calibrate the other comparison stars. T9 was meant to be a comparison star, but was out of the frame on a number of nights, so it was removed

Table A.5. ATLAS 4 V Filter Comparison Stars

Star	RA	Dec.	Magnitude	Std. deviation
C2	21:55:08.29	+58:00:42.76	12.09	n/a
(TYC 3976-208-1)				
C3	21:56:04.08	+58:03:47.62	12.34	n/a
(TYC 3976-69-1)				
C4	21:55:32.53	+57:56:29.08	13.365	0.021
C5	21:55:39.66	+57:57:06.00	12.521	0.012
C6	21:54:56.81	+57:57:27.74	12.405	0.012
C7	21:54:11.35	+58:04:45.14	12.702	0.020
C8	21:54:32.69	+58:03:33.92	12.702	0.017
C10	21:55:47.66	+58:07:59.85	13.331	0.020

Table A.6. Nights Observed for ATLAS 4

Date	Start Time (HJD)	End Time (HJD)	Length (hrs)	# Observations	Telescope
Sept 4, 2020	2459097.622929	2459097.992869	8.878560	111	10"
Sept 5, 2020	2459098.622012	2459098.999520	9.060192	145	10"
Sept 12, 2020	2459105.613034	2459106.022274	9.821760	155	10"
Sept 27, 2020	2459120.596031	2459121.015444	10.065912	160	10"
Sept 30, 2020	2459123.591494	2459124.005335	9.932160	160	10"
Oct 9, 2020	2459132.581051	2459132.723402	3.416424	111	12"
Oct 12, 2020	2459135.694204	2459135.756538	1.496016	50	12"
Oct 15, 2020	2459138.717904	2459138.905607	4.504872	150	12"
Oct 16, 2020	2459139.574009	2459139.921668	8.343816	122	10" and 12"
Oct 20, 2020	2459143.570466	2459143.867846	7.137120	234	12"
Oct 27, 2020	2459150.570324	2459150.850269	6.718680	217	12"
Oct 28, 2020	2459151.71484	2459151.957450	9.263184	340	10" and 12"
Oct 29, 2020	2459152.563159	2459152.715833	3.664176	40	10"
Oct 30, 2020	2459153.561575	2459153.716573	3.719952	75	10"
Nov 3, 2020	2459157.573375	2459157.685975	2.702400	88	12"
Nov 4, 2020	2459158.557973	2459158.900122	8.211576	259	10" and 12"
Nov 12, 2020	2459166.552542	2459166.882653	7.922664	262	10" and 12"
Dec 3, 2020	2459187.545934	2459187.816040	6.482544	124	10"
Dec 4, 2020	2459188.545898	2459188.805379	6.227544	130	10"
Dec 5, 2020	2459189.545861	2459189.785748	5.757288	120	10"
Dec 6, 2020	2459190.545825	2459190.795619	5.995056	125	10"
Dec 7, 2020	2459191.545788	2459191.795512	5.993376	125	10"
Dec 8, 2020	2459192.545751	2459192.799480	6.089496	127	10"
May 18, 2021	2459353.879960	2459353.924290	1.063920	36	12"
June 2, 2021	2459368.763791	2459368.912870	3.577896	118	12"
June 8, 2021	2459374.767477	2459374.911463	3.455664	114	12"
June 10, 2021	2459376.814773	2459376.910262	2.291736	76	12"
July 6, 2021	2459402.373133	2459402.750725	1.790208	60	12"
Aug 22, 2021	2459449.638964	2459449.710957	1.727832	58	12"
Aug 23, 2021	2459450.637351	2459450.730626	2.238600	75	12"

Table A.6 (cont'd)

Date	Start Time (HJD)	End Time (HJD)	Length (hrs)	# Observations	Telescope
Sept 23, 2021	2459481.819476	2459481.913822	2.264304	35	12"
Sept 26, 2021	2459484.711519	2459484.889528	4.272216	65	12"
Dec 3, 2021	2459552.546350	2459552.751550	4.924800	75	12"

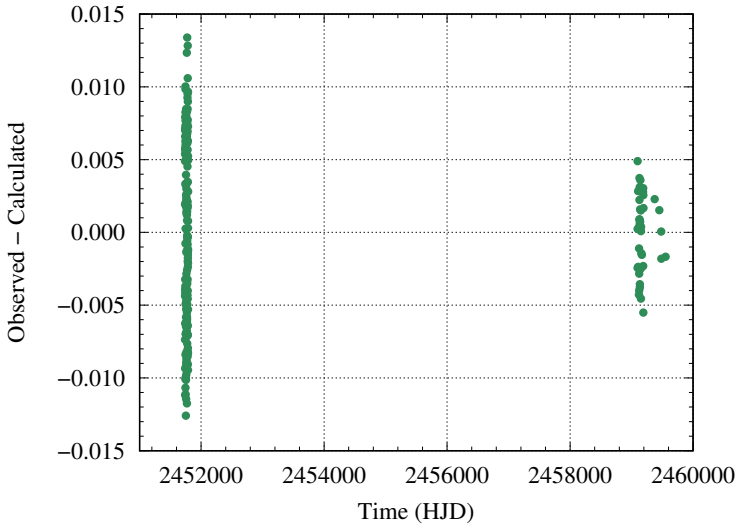

Figure A.5 O-C Diagram for ATLAS 4 from 231 times of maximum light. Note that the TESS times of maximum light were taken well before the BYU times, which is why there is a large gap

Table A.7. Frequency Content of ATLAS 4

Survey		Frequency c d^{-1}	Amplitude mag	S/N
	f_1	5.13745	0.13104	104.14965
BYU	$2f_1$	10.27479	0.02673	27.78468
(V filter)	f_2	2.00262	0.01277	5.27956
	f_3	6.42631	0.01314	11.59801
BYU	f_1	5.14008	0.15243	32.7112
(g filter)	$2f_1$	10.28015	0.02912	23.37278
BYU	f_1	5.13975	0.10737	25.65591
(R filter)	$2f_1$	10.27271	0.02160	13.8973
	f_1	5.13743	0.12347	56.15258
ASAS-SN	$2f_1$	10.27490	0.02422	10.95348
(V filter)	f_2	6.42640	0.01908	8.6778
	f_1	5.13748	0.14639	91.32268
ASAS-SN	$2f_1$	10.27498	0.02962	18.48925
(g filter)	f_2	6.42645	0.02430	15.21883
	f_3	11.56393	0.00906	5.62233
ATLAS	f_1	5.13745	0.12998	20.03852
(c filter)	$2f_1$	10.27534	0.03167	6.14785
ATLAS	f_1	5.13724	0.08537	8.78999
(o filter)				
	f_1	5.13773	0.06974	1019.70827
	f_2	6.42623	0.01751	322.13607
	$2f_1$	10.27444	0.01487	268.08525
	f_3	1.28952	0.00612	86.62106
	f_4	11.56396	0.00519	105.78782
	$3f_1$	15.41217	0.00406	89.5847
	f_5	16.70169	0.00291	77.07565
	f_6	7.71372	0.00166	35.40458
	f_7	3.84821	0.00156	29.77438
TESS	$4f_1$	20.54990	0.00092	20.78687
	f_8	21.83739	0.00088	19.02892

Table A.7 (cont'd)

Survey		Frequency c d^{-1}	Amplitude mag	S/N
	f_9	8.98492	0.00077	17.23871
	f_{10}	0.07124	0.00061	5.97999
	f_{11}	2.57802	0.00060	10.38554
	f_{12}	7.43587	0.00050	9.59889
	f_{13}	9.48872	0.00048	9.33858
	f_{12}	7.40940	0.00042	7.90554
	f_2	6.58297	0.00043	8.10076
	f_{14}	9.83578	0.00040	7.23408
	f_{15}	17.99020	0.00038	9.12544
	f_{16}	13.14151	0.00036	6.81445

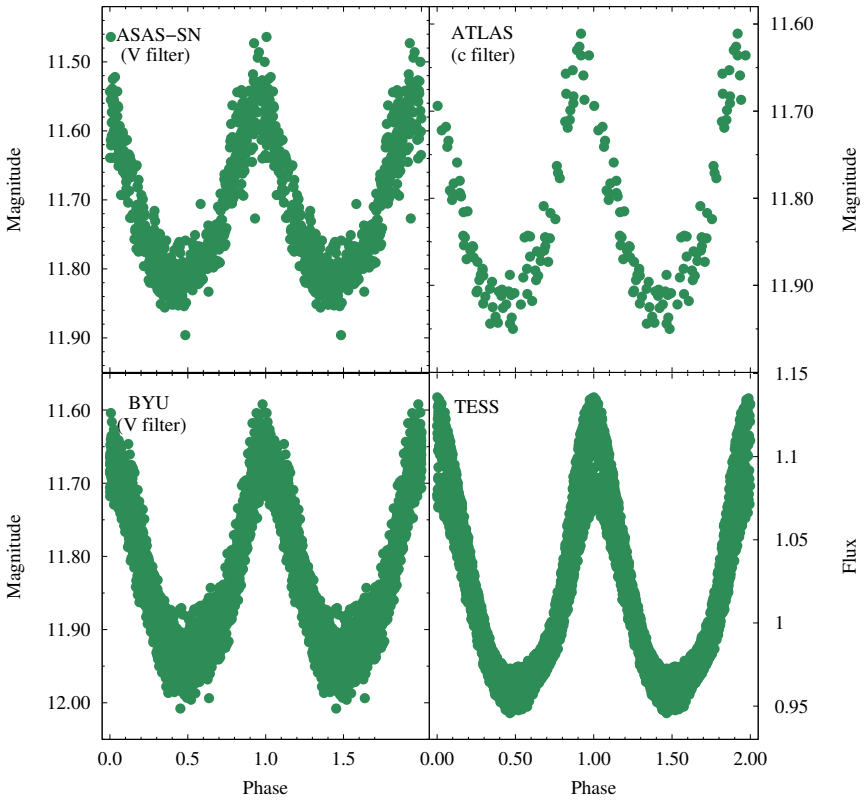

Figure A.6 Phased Data for ATLAS 4 from BYU, ATLAS, ASAS-SN, and TESS using the calculated period

A.3 ATLAS 8

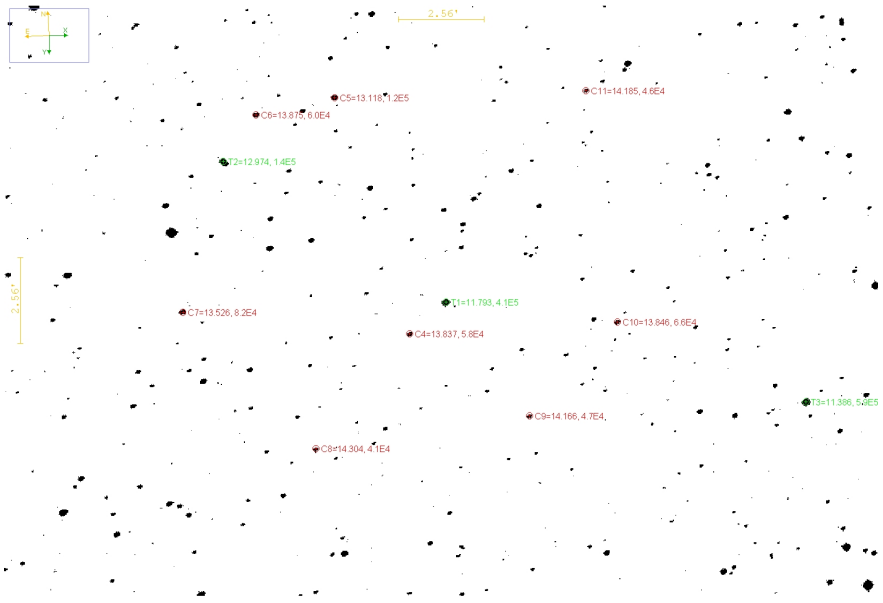

Figure A.7 Field of ATLAS 8 (labeled T1) with comparison stars C4-C11. T2 and T3 were used, along with C4, to calibrate the other comparison stars.

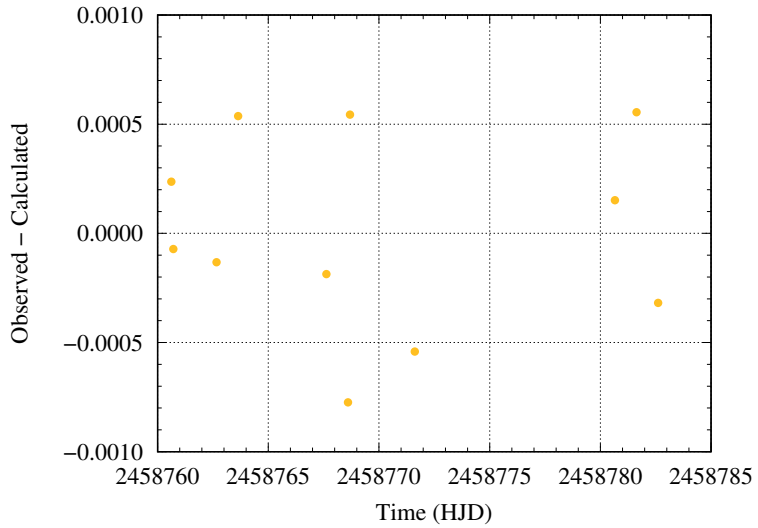

Figure A.8 O-C Diagram for ATLAS 8 from 13 times of maximum light. Note that the AAVSO data is not included here since it happens significantly before the other data points

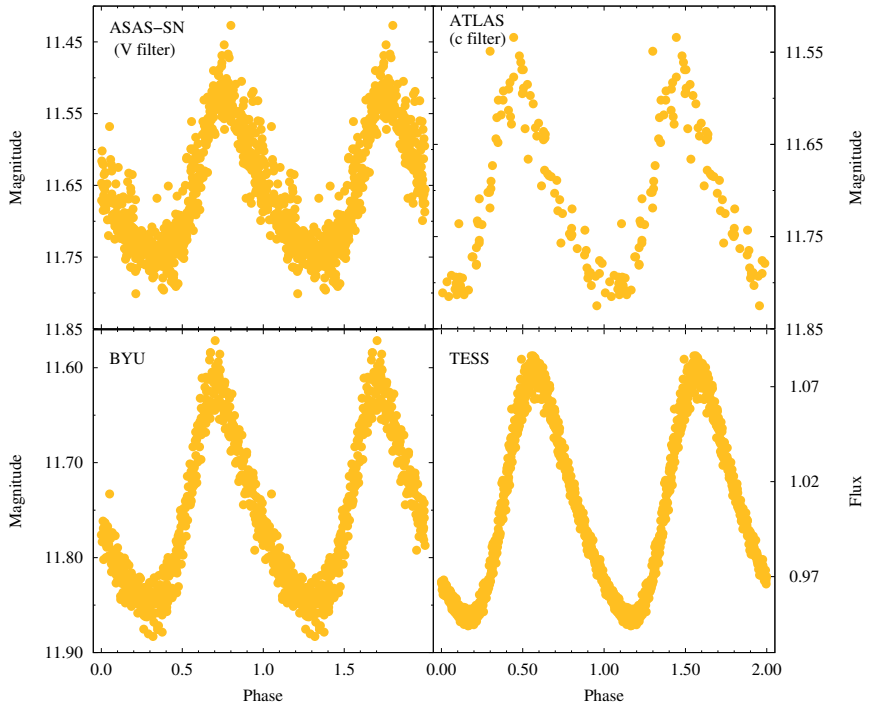

Figure A.9 Phased Data for ATLAS 8 from BYU, ATLAS, ASAS-SN, and TESS using optimal periods from each survey

Table A.8. ATLAS 8 Comparison Stars

Star	RA	Dec.	V	σ_m
T2	03:03:36.64	+45:58:51.43	12.48	n/a
(TYC 3224-3300-1)				
T3	03:03:36.64	+45:58:51.43	11.41	n/a
(TYC 3224-359-1)				
C4	03:02:16.03	+46:01:03.98	13.837	0.003
C5	03:03:37.52	+46:02:15.96	13.118	0.001
C6	03:03:19.95	+45:55:08.89	13.875	0.002
C7	03:02:38.21	+45:57:10.60	13.526	0.001
C8	03:02:45.87	+45:58:58.75	14.304	0.003
C9	03:02:39.19	+46:05:27.20	14.166	0.002
C10	03:03:44.18	+46:02:59.67	13.846	0.002
C11	03:03:44.18	+46:02:59.67	14.185	0.002

Table A.9. Times of Maximum Light for ATLAS 8

Cycle	HJD 2450000.0+	$O-C$	Source
-12374	7663.57195	-0.00001	AAVSO
-12373	7663.66064	0.00003	AAVSO
0	8760.62169	-0.00003	BYU
1	8760.71004	-0.00034	BYU
23	8762.66050	-0.00034	BYU
34	8763.63644	0.00036	BYU
79	8767.62542	-0.00025	BYU
90	8768.60009	-0.00081	BYU
91	8768.69007	0.00051	BYU
124	8771.61477	-0.00049	BYU
226	8780.65881	0.00046	BYU
237	8781.63447	0.00089	BYU
248	8782.60886	0.00005	BYU

Table A.10. Frequency Content of ATLAS 8

Survey		Frequency c d^{-1}	Amplitude mag	S/N
BYU	f_1	11.27773	0.10765	44.8
(V filter)	$2f_1$	22.55772	0.02651	21.8
ASAS-SN	f_1	11.27847	0.10831	56.3
(V filter)	$2f_1$	22.55690	0.02601	13.6
	f_1	11.27848	0.12250	92.0
ASAS-SN	$2f_1$	22.55689	0.02960	22.2
(g filter)	$3f_1$	33.83541	0.01002	7.9
	f_2	2.00280	0.00840	6.1
ATLAS	f_1	11.27851	0.10677	20.8
(c filter)	$2f_1$	22.55691	0.02501	5.7
ATLAS	f_1	11.27833	0.07790	23.8
(o filter)	$2f_1$	22.55695	0.02093	7.5
	f_1	11.27699	0.06113	149.3
TESS	$2f_1$	22.55529	0.01195	78.4
	$3f_1$	36.62712	0.00284	6.8

A.4 ATLAS 63

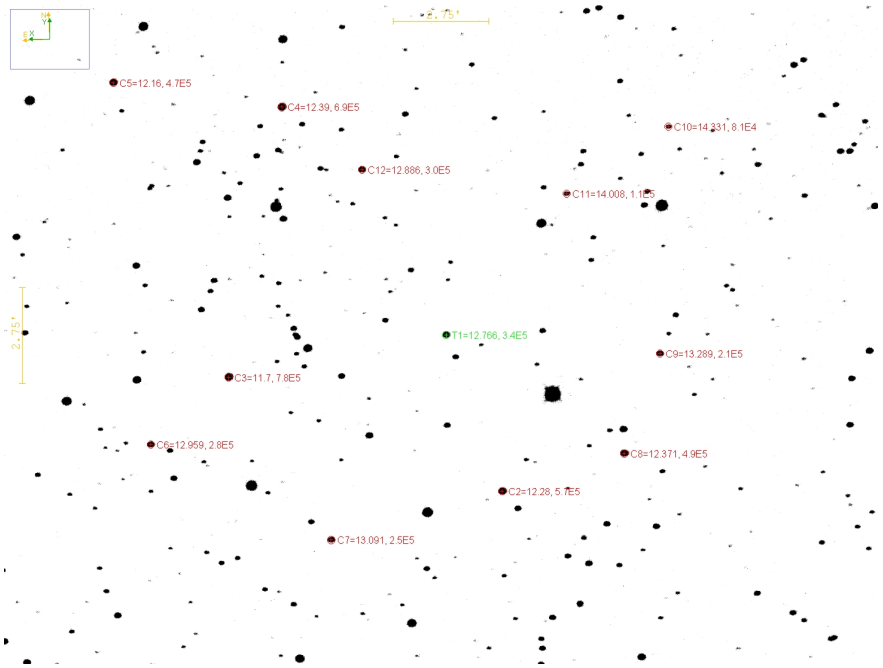

Figure A.10 Field of ATLAS 63 (labeled T1) with comparison stars C2-C12. C2-C5 were used to calibrate the other comparison stars.

Table A.11. ATLAS 63 V Filter Comparison Stars

Star	RA	Dec.	Magnitude	Std. deviation
C2 (TYC 2401-256-1)	05:10:19.19	+36:29:10.22	12.28	n/a
C3 (TYC 2401-1181-1)	05:10:57.49	+36:32:47.54	11.70	n/a
C4 (TYC 2401-1032-1)	05:10:48.22	+36:40:27.75	12.39	n/a
C5 (TYC 2401-684-1)	05:11:12.16	+36:41:22.46	12.16	n/a
C6	05:11:09.12	+36:30:57.35	12.959	0.012
C7	05:10:43.95	+36:27:59.84	13.091	0.013
C8	05:10:01.56	+36:30:05.79	12.371	0.008
C9	05:09:55.81	+36:32:54.29	13.289	0.012
C10	05:09:53.08	+36:39:23.83	14.331	0.023
C11	05:10:08.11	+36:37:36.78	14.008	0.021
C12	05:10:37.21	+36:38:34.16	12.886	0.008

Table A.12. Nights Observed for ATLAS 63

Date	Start Time (HJD)	End Time (HJD)	Length (hrs)	# Observations
March 5, 2020	2458914.612454	2458914.736872	2.986032	45
March 10, 2020	2458919.619979	2458919.713683	2.248896	30
Dec 4, 2020	2459188.876007	2459189.024399	3.561408	65
Dec 5, 2020	2459189.888512	2459190.025411	3.285576	60
Dec 6, 2020	2459190.934350	2459191.024709	2.168616	40
Dec 7, 2020	2459191.964213	2459192.045278	1.945560	36
Dec 3, 2021	2459552.886419	2459553.011015	2.990304	55
Feb 7, 2022	2459618.580783	2459618.637325	1.357008	25
Feb 8, 2022	2459619.582780	2459619.656244	1.763136	31

Table A.13. Times of Maximum Light for ATLAS 63

Cycle	HJD 2450000.0+	$O-C$	Filter
0	8914.65655	0.00131	V
71	8919.64328	-0.00166	V
2721	9105.88106	0.00041	R
2722	9105.95036	-0.00056	R
2892	9117.89688	-0.00124	R
2893	9117.96746	-0.00094	R
2935	9120.92003	-0.00003	R
2950	9121.97503	0.00081	R
3262	91443.8998	-0.00105	R
3591	9167.02270	0.00052	R
3875	9186.98099	-0.00004	R
3903	9188.94845	-0.00034	V
3917	9189.93317	0.00048	V
3918	9190.00289	-0.00007	V
3932	9190.98705	0.00020	V
3946	9191.97397	0.00324	V
9082	9552.91483	-0.00179	V
9083	9552.98559	-0.00130	V
10017	9618.62658	0.00038	V
10031	9619.61173	0.00165	V

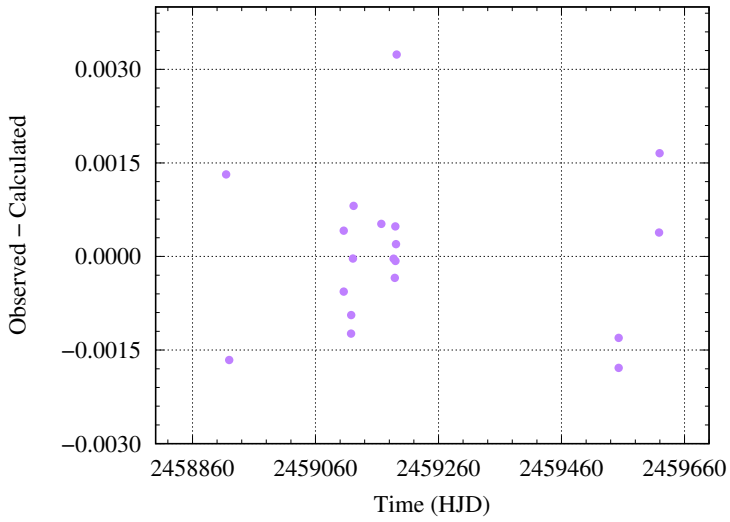

Figure A.11 O-C Diagram for ATLAS 63 from 19 times of maximum light.

Table A.14. Frequency Content of ATLAS 63

Survey		Frequency c d^{-1}	Amplitude mag	S/N
BYU	f_1	14.22933	0.05219	65.98345
(V filter)	$2f_1$	27.46702	0.01168	13.93366
ASAS-SN	f_1	14.22930	0.053008	25.74545
(V filter)	$2f_1$	28.45870	0.01321	6.444
ASAS-SN	f_1	14.22933	0.06195	32.23289
(g filter)	$2f_1$	28.45863	0.01492	7.8312
ATLAS	f_1	14.22933	0.05362	29.26738
(c filter)	$2f_1$	28.45863	0.01151	6.59939
	f_2	13.22086	0.00817	5.71185
ATLAS	f_1	14.22929	0.03724	19.77387
(o filter)	$2f_1$	27.45600	0.00988	6.28471
	f_1	14.22678	0.02395	181.0264
TESS	$2f_1$	28.45413	0.00346	32.56933
	f_2	48.07240	0.00147	5.62483

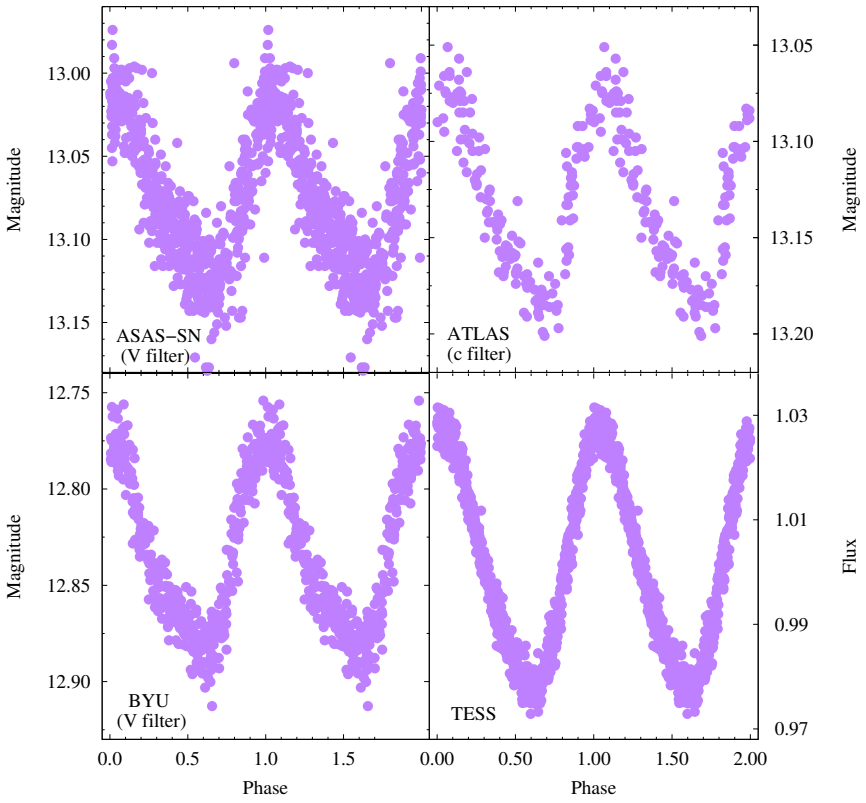

Figure A.12 Phased Data for ATLAS 63 from BYU, ATLAS, ASAS-SN, and TESS using the calculated period

A.5 ATLAS 75

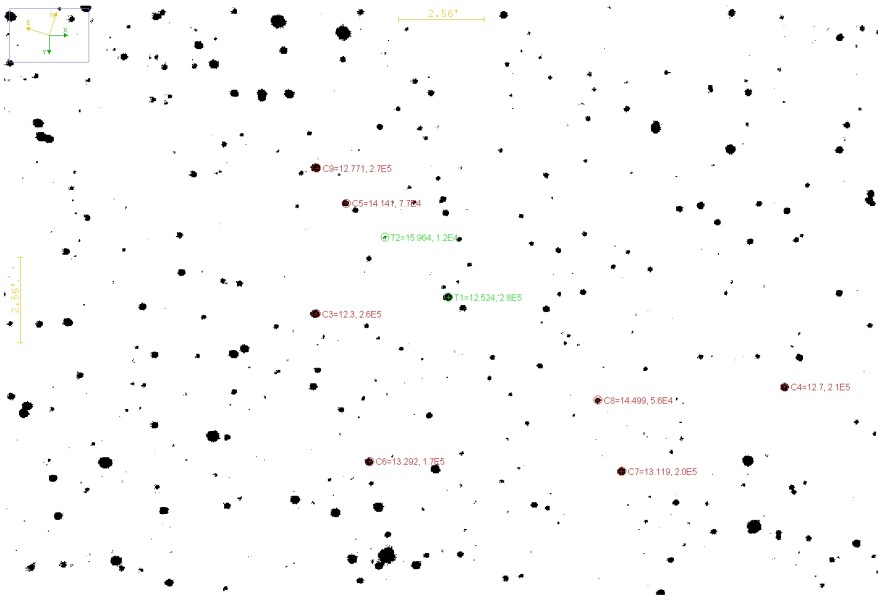

Figure A.13 Field of ATLAS 75 (labeled T1) with comparison stars C3-C10. T2 is another variable star and was not used as a comparison star.

.

Table A.15. ATLAS 75 V Filter Comparison Stars

Star	RA	Dec.	V	σ_m
C3	03:03:36.64	+45:58:51.43	12.3	n/a
(2MASS J03033664+4558514)				
C4	03:02:16.03	+46:01:03.98	12.7	n/a
(2MASS J03021602+4601040)				
C5	03:03:37.52	+46:02:15.96	14.141	0.007
C6	03:03:19.95	+45:55:08.89	13.292	0.005
C7	03:02:38.21	+45:57:10.60	13.119	0.004
C8	03:02:45.87	+45:58:58.75	14.509	0.008
C9	03:02:39.19	+46:05:27.20	13.525	0.004
C10	03:03:44.18	+46:02:59.67	12.771	0.004

Table A.16. Times of Maximum Light for ATLAS 75

Cycle	HJD 2450000.0+	$O-C$
0	8726.96627	0.00080
10	8727.81937	-0.00156
11	8727.90635	-0.00012
22	8728.84821	0.00074
23	8728.93406	0.00104
162	8740.82170	-0.00220
163	8740.90989	0.00044
220	8745.78401	-0.00156
221	8745.86903	-0.00208
222	8745.95913	0.00247
255	8748.78062	0.00095
256	8748.86522	-0.00000
257	8748.95183	0.00107

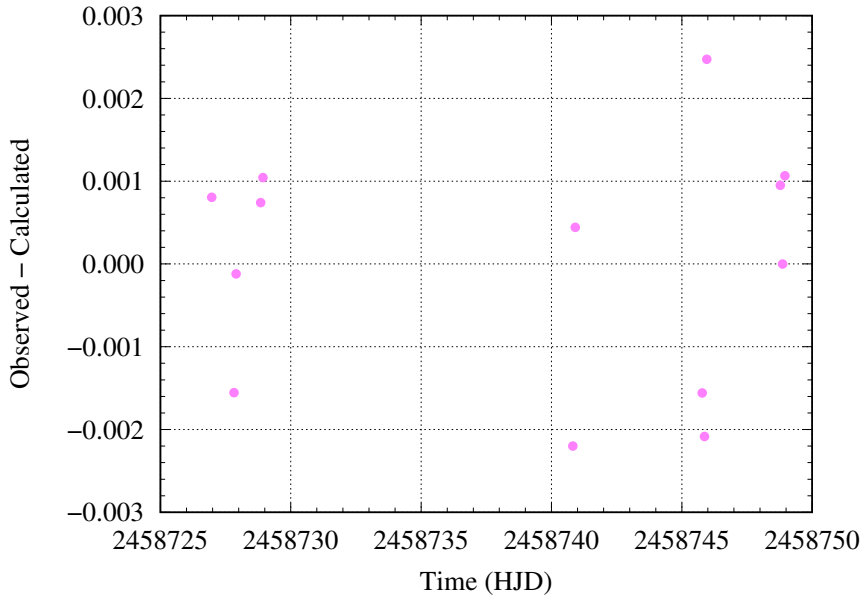

Figure A.14 O-C Diagram for ATLAS 75 from 13 times of maximum light.

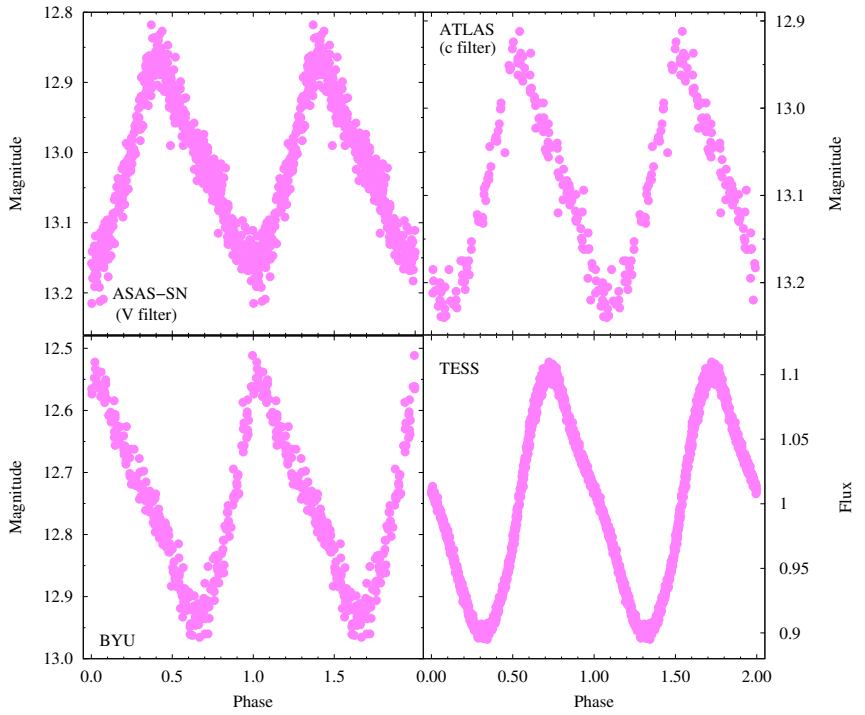

Figure A.15 Phased Data for ATLAS 75 from BYU, ATLAS, ASAS-SN, and TESS using optimal periods for each survey

Table A.17. Frequency Content of ATLAS 75

Survey		Frequency c d^{-1}	Amplitude mag	S/N
BYU	f_1	11.69009	0.16330	57.6
(V filter)	$2f_1$	23.38018	0.04374	31.8
	$3f_1$	35.02047	0.01204	4.8
	f_1	11.69005	0.12894	83.8
ASAS-SN	$2f_1$	23.38006	0.02537	16.1
(V filter)	f_2	13.69218	0.01019	6.9
	$3f_1$	34.06738	0.00831	5.7
	f_1	11.68990	0.17171	102.6
ASAS-SN	$2f_1$	23.37975	0.05188	32.0
(g filter)	$3f_1$	35.06961	0.01571	9.3
	$4f_1$	46.75958	0.00861	5.4
ATLAS	f_1	11.69004	0.12616	58.9
(c filter)	$2f_1$	23.38007	0.01999	9.7
	$3f_1$	35.07020	0.01056	5.4
ATLAS	f_1	11.69015	0.09045	24.8
(o filter)	$2f_1$	23.28019	0.01606	6.8
	f_1	11.68931	0.09360	722.0
	$2f_1$	23.37788	0.01897	179.8
TESS	$3f_1$	35.06686	0.00430	43.8
	f_2	14.58322	0.00237	23.7
	f_3	2.89239	0.00172	13.9
	f_4	10.44874	0.00112	11.3

Bibliography

Amôres, E. B., et al. 2021, MNRAS, 508, 1788

Bailer-Jones, C. A. L., Rybizki, J., Fouesneau, M., Demleitner, M., & Andrae, R. 2021, VizieR Online Data Catalog, I/352

Breger, M. 1979, PASP, 91, 5

Breger, M. 1990, Delta Scuti Star Newsletter, 2, 21

Breger, M., & Pamyatnykh, A. A. 1998, Astron. Astrophys., 332, 958

Carroll, B. W., & Ostlie, D. A. 2017, An Introduction to Modern Astrophysics, 2nd edn. (Cambridge University Press)

Christy, C. T., et al. 2023, MNRAS, 519, 5271

Collins, K. A., Kielkopf, J. F., Stassun, K. G., & Hessman, F. V. 2017, AJ, 153, 77

Heinze, A. N., et al. 2019, VizieR Online Data Catalog, J/AJ/156/241

Hintz, E. G., Hansen, J. L., Stephens, D. C., & Derieg, B. J. 2022, Journal of the American Association of Variable Star Observers, 50, 192

Jenkins, J. M., et al. 2016, in Society of Photo-Optical Instrumentation Engineers (SPIE) Conference Series, Vol. 9913, Software and Cyberinfrastructure for Astronomy IV, ed. G. Chiozzi & J. C. Guzman, 99133E

Kochanek, C. S., et al. 2017, PASP, 129, 104502

Lenz, P., & Breger, M. 2005, Communications in Asteroseismology, 146, 53

Paunzen, E., & Vanmunster, T. 2016, Astronomische Nachrichten, 337, 239

Poro, A., et al. 2021, PASP, 133, 084201

Ricker, G. R., et al. 2015, Journal of Astronomical Telescopes, Instruments, and Systems, 1, 014003

Rodríguez, E., López-González, M. J., & López de Coca, P. 2000, A&AS, 144, 469

Shappee, B. J., et al. 2014, ApJ, 788, 48

Index